4

Characterizing Functionalized Carbon Nanotubes for Improved Fabrication in Aqueous Solution Environments

Charles C. Chusuei and Mulugeta Wayu
Chemistry Department, Middle Tennessee State University, Murfreesboro
USA

1. Introduction

The rediscovery of carbon nanotubes (Iijima, 1991) has inspired extensive research activity. These materials have extremely high surface areas, large aspect ratios, remarkably high mechanical strength, and can have electrical and thermal conductivities that are similar to that of copper (Ebbesen et al., 1996). They come in two forms: single-walled carbon nanotubes (SWNTs) and multiwalled carbon nanotubes (MWNTs). SWNTs have diameters ranging from 1.2 to 1.4 nm. MWNTs have larger overall diameters, with sizes depending on the number of concentric walls within the structure. Like graphite, carbon nanotubes are relatively non-reactive, except at the nanotube caps which are more reactive due to the presence of dangling bonds. The reactivity of the carbon nanotube side walls' π-system can also be influenced by tube curvature or chirality (Okpalugo et al., 2005). In particular, their remarkable structure-dependent properties have attracted great attention due to their potential applications in heterogeneous catalysis (Planeix et al., 1994), use as substrates for destruction of cancer cells (Kam et al., 2005) and applications for biological and chemical sensing (Poh et al., 2004). Carbon nanotubes require chemical modification in aqueous solution environments to make them more amenable for attachment of reactive surface species. In the case of attaching metal nanoparticles to the carbon surface, functionalization is necessary to avoid agglomeration of the metal. Sensor applications involve the tethering of chemical moieties with specific recognition sites for the detecting ultra-trace analytes (Dai, 2002). Surface functionalization is also necessary for depositing high-loading, catalytically active metal nanoparticles on them (Xing et al, 2005).

Great attention has been paid to attaching functional groups onto carbon nanotube surfaces (Holzinger et al., 2001; Kim et al., 2004; Chen et al., 2005; Park et al., 2006) and probing the electronic structure resulting from post-nanotube-synthesis preparations. To understand the changes that result from surface functionalization strategies, well-defined characterization of the carbon nanotube's surface chemistry and structure is needed. The ability to get an accurate detailed picture of the tethered functional groups that attach to the solid surface using aqueous solution preparation methods is important for controlling carbon nanotube surface composition composition.

We have developed an array of analytical methods to probe the surface composition of carbon nanotubes during various stages of nanomaterial synthesis in our laboratory. Summarized herein are three case studies. In the first study, sonochemically functionalized MWNTs were probed by X-ray photoelectron spectroscopy (XPS) revealing a consecutive, first-order attachment mechanism. In the second study, extended X-ray absorption fine structure (EXAFS) and attenuated total reflection infrared (ATR-IR) spectroscopy were used to examine tethered Pt nanoparticles on functionalized MWNTs. In the third study, we functionalized high pressure carbon monoxide (HiPco) SWNTs to produce carboxylic acid (COOH-SWNT), maleic anhydride (MA-SWNT), and nitroso (NO-SWNT) attached SWNTs in order to examine the effects of the tethered groups on the solid surface point-of-zero charge (PZC). The PZC is defined as the aqueous solution pH value at which the degree of surface protonation and hydroxylation are equal, which results in an electrostatically neutral charge at the electrical double layer interface (Brown et al., 1999). SWNTs were used in the PZC studies due to their relative ease for surface functionalization with specific moieties.

2. Experimental

In the first case study, MWNTs produced from chemical vapor deposition were obtained from Nanolab, Inc. (Waltham, MA). The as-purchased MWNTs (95% purity, ~30 nm in diameter) were put into a mixture solution of HNO_3 and H_2SO_4 in an Erlenmeyer flask. The concentrations of both acids were 8.0 M. The flask was placed in an ultrasonic bath (Fisher Scientific, 130 W and 40 kHz) maintained at 60 °C. Sonication was performed for 1, 2, 4 and 8 hrs. The sonochemically treated MWNTs were then separated from the acids in a centrifuge (Thermal IEC Centra CL2), and thoroughly washed using doubly distilled, deionized water prior to analysis (Xing et al., 2005).

The chemical oxidation states and surface compositions of the resulting sonochemically treated MWNTs and Pt electrocatalysts were analyzed by XPS using an ion-pumped Perkin-Elmer PHI ESCA 560 system using a PHI 25-270AR double pass cylindrical mirror analyzer. An Mg Kα anode operated at 15 kV and 250 W with photon energy of $h\nu$= 1253.6 eV was used. The base pressure of the chamber after a bake out was ~$1x10^{-10}$ Torr. The operating pressure during XPS scans did not exceed $5x10^{-8}$ Torr. The C 1s core level at 284.4 eV, corresponding with the carbon nanotube oxidation state (Suzuki et al., 2002), was used to charge reference the XP spectra. XPS data were curve fitted using CasaXPS VAMAS processing software version 2.2 (Devon, United Kingdom) with a Shirley background subtraction and 70%-to-30% Gaussian-Lorentzian line shapes.

In the second case study, MWNT-Pt nanoparticle structural analysis was performed using EXAFS. Finely dispersed Pt nanoparticles (3.5 nm in diameter) tethered onto MWNTs were prepared via sonicating MWNTs in HNO_3/H_2SO_4 for 2 hrs followed by reducing the Pt salt precursor, K_2PtCl_4 (Xing, 2004). Spectra were obtained from the 12-BM BESSRC Advanced Photon Source (APS) beamline at the Argonne National Laboratory and the X18B beamline at the National Synchrotron Light Source (NSLS) at the Brookhaven National Laboratory to analyze the Pt L_{III} edge (11.564 keV) of the Pt nanoparticles tethered to the carbon nanotube surface. A spectrum of a 5 μm thick Pt foil was taken in the transmission mode for absolute energy calibration. The absorption edge of the data obtained for each sample, plotted as χ

(*E*), was checked to ensure alignment prior to plotting in *k* space. Spectra of the dried MWNT-Pt nanoparticles samples and PtO_2 standard were obtained in the fluorescence mode. Anhydrous PtO_2 (99.95% purity, metals basis) obtained from Alfa Aesar, 8 mg of which were diluted in 170 mg of boron nitride, was used as received for the reference spectrum. In the beamline, a double crystal Si (111) monochromator was used for energy selection. Spectra taken in the fluorescence mode used a 13-element Ge detector. The ion chambers employed had a 8:2 gas mixture of N_2-to-Ar. Data were processed using the IFEFFIT library of numerical XAS algorithms written in Perl programming that utilizes the *ab initio* EXAFS code, FEFF 6.01 (Newville, 2001; Ravel et al., 2005). Further analysis by ATR-IR and Raman spectroscopies were performed as described by Hull et al. (2006).

The experimental procedure for the third case study (McPhail et al., 2009) was as follows: (1) COOH-SWNTs were prepared by refluxing in H_2SO_4/HNO_3 according to Lu et al. (2007). A 30.0 mL solution of 3:1 concentrated nitric-to-sulfuric acid ratio was added to a 100-mL round-bottom glass flask along with 60.1 mg of p-SWNTs. The mixture was refluxed at 338 K for 12 hrs, with constant magnetic stirring, under N_2 atmosphere. (2) NO-SWNTs were prepared using an electrochemical functionalization procedure based on the description made by Wang et al. (2005). SWNT sheets were prepared by sonicating them in 1% Triton X-100 (The Chemistry Store.com Inc.; St. Cayce, SC) solution followed by vacuum filtration with Millipore Teflon filter paper (0.2 μm pore size). The solid was dried on the filter paper and lifted off as a single sheet to be used as a working electrode in the electrochemical functionalization. Remaining surfactant was removed by annealing at 120 °C for 2 hrs, 300 °C for 1 hr, and 800 °C for 30 minutes under inert Ar atmosphere. Complete removal of the Triton X-100 required additional electrochemical oxidation of the nanotubes, which occurred during the nitrosylation. Electrochemical nitrosylation took place in 6 M KNO_2 with a SWNT sheet as the working electrode, AgCl as the reference electrode, and Pt wire as the counter electrode. The system was sparged with Ar gas and run for 6 hrs at 2.0 V using a 273 EG&G Princeton Applied Research potentiostat. (3) The MA-SWNTs adduct was prepared via Diels-Alder addition reaction with maleic anhydride as the dienophile (Dewar et al., 1970), in good agreement with *ab initio* predictions for Diels-Alder additions to SWNT sidewalls (Mercuri et al., 2009). The synthesis involved adding 50.0 mg of the HiPco p-SWNTs to an excess of maleic anhydride dissolved in chloroform. This mixture was placed in a 100-mL round-bottom flask and refluxed at 323 K for 12 hrs, with constant stirring, under N_2 atmosphere. All of the functionalization procedures were carried out for prolonged periods (12 hrs) to ensure saturation of the SWNTs with their respective moieties. The SWNTs were then recovered by vacuum filtration using a Buchner funnel and Fluoropore polytetrafluoroethylene (PTFE) membrane filters with a 0.2 μm pore size. Samples were rinsed with copious amounts of Millipore H_2O. Samples were then dried in a vacuum desiccator and saved in glass vials for further analysis.

Isoelectric point measurements at the solid-liquid interface were made on MA-SWNT, NO-SWNT, COOH-SWNT and p-SWNT surfaces using a method described by Park and Regalbuto (1995). Twelve solutions in the range of pH = 1.0-12.0 were made using dilute aqueous solutions of NaOH and HCl. A 1.8 mL aliquot of each solution was pipetted into polyethylene vials and allowed to equilibrate for 1 hr. The initial pH of each solution was then recorded. A 2.0 mg amount of the SWNTs to be examined were added to each vial, which were then capped and shaken with a vortex mixer to settle the SWNTs. After an additional 12-hr equilibration period, the final pH at the SWNT solid surface was measured

for each vial using a spear-tip semisolid electrode. Finally, initial pH values versus final pH values were plotted.

3. Results and discussion

The sonochemically functionalized MWNTs were characterized and quantified by XPS. XPS is an effective surface sensitive method for quantifying the extent (or level) of surface oxidation (Huefner, 2003). The distribution of oxygen containing functional groups (-C-O-, -C=O, and O-C=O) is also often characterized by deconvoluting the C 1s spectral envelope to obtain quantitative information, based on differences in XPS binding energy (BE) (Datsyuk et al., 2008).

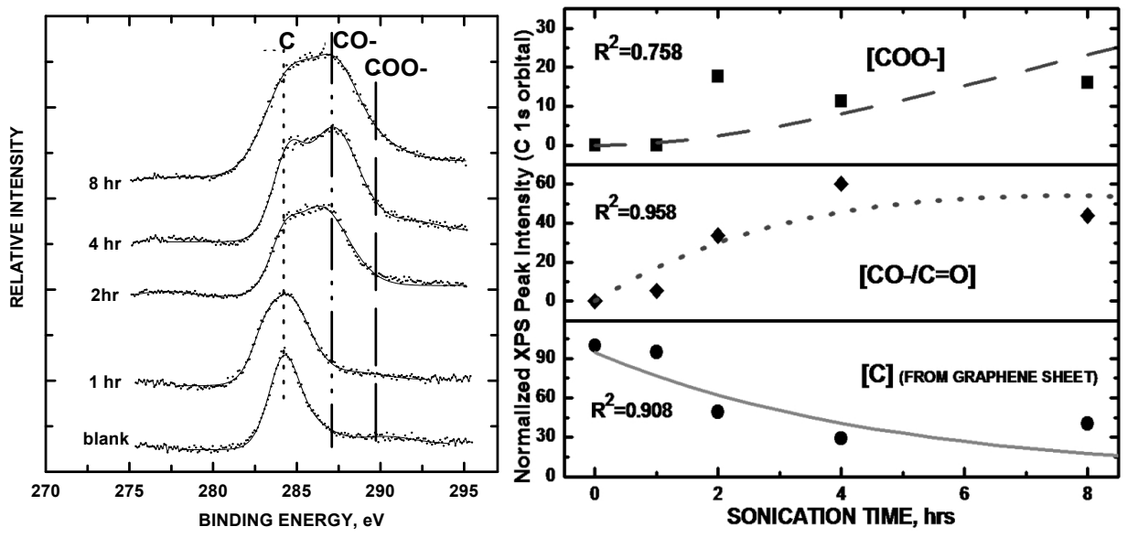

Fig. 1. (Left-hand panel) XPS stackplot of C 1s core level of the carbon nanotubes at varying sonochemical treatment times; (Right-hand panel) Kinetic model of sonochemically treated carbon nanotube oxidation process based on deconvoluted XPS C 1s integrated peak areas for C (on the MWNT graphene sheet), CO- and COO- oxidation states.

Fig. 1 (left-hand panel) shows the narrow scan spectra of the C 1s region of sonochemically treated and untreated MWNTs. The XPS spectrum shows distinct carbon peaks, representing the major constituents of the oxidized MWNT surface. The dominant peak structure for the C 1s core level at a BE of 284.4 eV corresponds to the bare, untreated MWNT surface (Ago et al., 1999; Suzuki et al., 2002). C 1s core level shifts at 287.6 and 288.3 eV indicate that the moieties consist of CO-/C=O and COO- respectively, in agreement with literature values reported for these groups tethered onto the MWNTs (Langley et al., 2005). Intensities of the high BE states increased due to oxidation as sonication ensued. The CO-/C=O and COO- concentrations were quantified relative to the graphitic carbon peak. The C 1s line broadening with extra feature developments were attributed to the surface oxidation of MWNTs where C atoms bond to more O atoms as a result of the sonochemical treatment. The population of the oxidized groups (CO-, C=O, and COO-) relative to the MWNT carbon were quantified via plotting the sum of their C 1s peak areas relative to that of the graphitic MWNT carbon as a function of sonochemical treatment time. The increase in

surface oxidation measured from the integrated C 1s peak areas of the ([CO-] + [COO-])/[C] tracks well with the overall increase in XPS atomic percent oxygen. A greater uptake of oxygen by the surface carbon atoms corresponds to a higher population density of CO_x functional groups detected by the XPS.

The kinetic model for the oxidation process is shown in Fig. 1 (right-hand panel). A stochastic addition mechanism obeying a consecutive 1st-order mechanism was revealed. Here, we report the first detailed mechanistic delineation of the carbon nanotube oxidation process. Evolution of the high binding energy peak intensities during sonication shows a consecutive, single-step first order O-attachment mechanism, leading to the carboxylate. This scheme is consistent with a report made by (Chiang et al., 2011) showing CO to be an intermediate species, which could be oxidized quickly to other forms, usually COO under acidic environment. Sonication creates defect sites on the sidewalls that allow for O atom attachment (Li et al., 2006). Differential equations describing the mechanism are as follows:

$$\frac{d[C]}{dt} = -k_1[C]; \frac{d[CO-]}{dt} = k_1[C] - k_2[COO]; \frac{d[COO]}{dt} = k_2[CO].$$

Least squares fittings show rate constants of k_1 (C→CO) = 2.11(±0.15) x10^{-2} s^{-1} and k_2 (CO→COO) = 7.3(±1.2) x10^{-2} s^{-1}. The overall correlation coefficient (R^2) value = 0.923 indicated the goodness of fit for our kinetic model. R^2 values for individual concentration profiles of C, CO and COO are shown in Fig. 1 (right-hand panel). We thus demonstrate that stochastic functionalization on MWNTs is possible under aqueous solution conditions. In contrast, gas phase kinetic studies have typically been limited to a single-step reaction (Brukh et al., 2007).

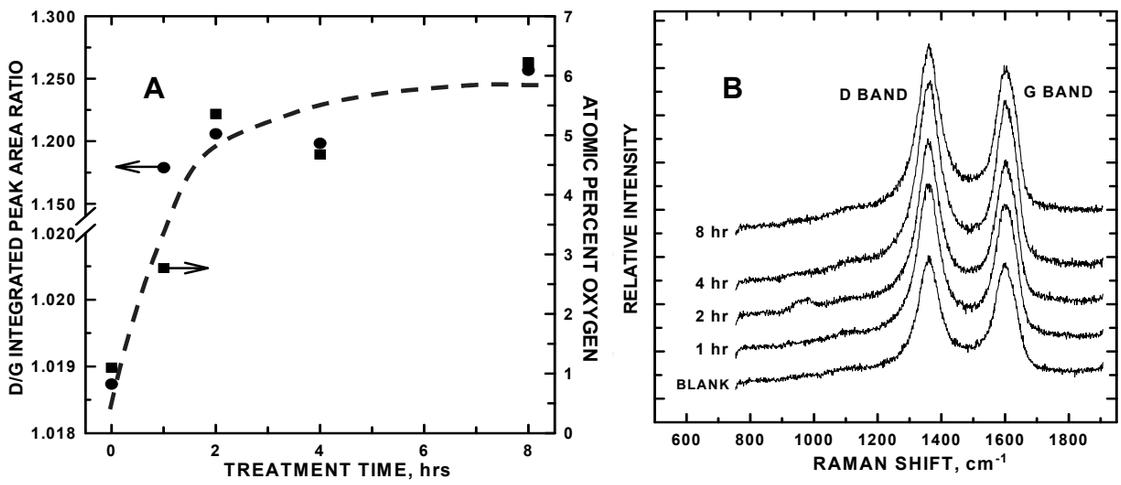

Fig. 2. (A) A plot of the uptake of D-to-G integrated peak area ratios (●, left-hand axis) and atomic percent oxygen (■, right-hand axis) versus sonochemical treatment time; (B) Raman shifts showing the emergence of the D and G bands of sonochemically treated MWNTs before deposition of Pt nanoparticles. The dashed line serves as a guide to the eye, denoting functional group saturation at 2 hrs.

In examining the Raman D-to-G integrated peak area ratios (Fig. 2A; left-hand axis), the disordered sp^3 state increased with longer sonochemical treatment. The largest increase

occurred between 0 and 1 hr of sonication with a plateau reached at 2 hrs. Noteworthy is the fact that the plateau of the relative Raman D-to-G band intensities (left-hand axis) coincided with a plateau of the atomic percent mole fractions of oxygen (right-hand axis), obtained from normalizing XPS high-resolution energy scans of the O 1s core level (Fig. 2A; right-hand axis), at 2 hrs. The population of sp^3-hybridized carbon increased relative to the sp^2-hybridized carbon during sonication, accompanying the creation of sidewall defects to which the functional groups attached. Thus, the groups covalently bonded to the surface with moieties directly forming from C atoms within the graphene sheets. The growth rate of sp^3-to-sp^2 Raman intensities with sonication time (Fig. 2B) was also consistent with that of our consecutive 1st-order kinetic model. The density of the surface functional groups was directly (albeit not linearly) related to sonication time; 2 hrs of sonication resulted in optimal Pt nanoparticle dispersion. Upon deposition of the Pt nanoparticles, the Raman line shapes and relative D-to-G band intensities remained unchanged. The presence of these peaks verified that the carbon nanotubes remained largely intact during the oxidation procedure and after deposition of Pt nanoparticles.

To examine the local structure of the nanoparticles, EXAFS was performed on the Pt deposited on the 2-hr sonochemically treated carbon nanotubes. The Pt-CNT samples were examined as a dry powder-like form instead of aqueous solution phase to get a stronger signal. EXAFS is an oscillatory feature in the X-ray absorption above the absorption edge of the target atoms and is defined as the fraction deviation in the absorption coefficient:

$$\chi(k) = \sum \frac{N_j f_j(k) \exp[-2k^2 {\sigma_j}^2]}{k {R_j}^2} \sin[2kR_j + \delta_j(k)]$$

with R being the distance from the target to neighboring atom. N is the coordination number of the neighboring atom, and σ^2 is the disorder of the neighbor distance (i.e., the Debye-Waller factor). The photoelectron wave number $k = [2m\,(E-E_o)/\hbar^2]^{1/2}$, $f(k)$ is the scattering amplitude, and $\delta(k)$ is the phase shift. Oscillations arise from the photoelectron wave backscattering from the nearest neighbor atoms. Assuming a cuboctahedron structure, predicted for the Pt nanoparticles of the size (3.5 nm in diameter) deposited on a carbon surface, there would be ~1500 atoms per cluster on the 20% Pt loaded, 2-hr sonochemically treated MWNT surface. Though the majority of the bonding emanated from bulk Pt-Pt interactions according to XPS (*vide infra*), EXAFS oscillations indicate Pt coordination to lower molecular weight atoms. The only two low-molecular-weight atoms present that can interact with Pt are C and O. The formation of Pt-C in the cluster was unlikely because temperatures in excess of 560°C are required to form the carbide (Kojima et al., 1982; Lamber et al., 1993). Since EXAFS scattering is sensitive only to the first few atomic shells and given the size of the Pt NPs, PtO_x appears to be present only at the top most surface layers of the cluster. A majority of the Pt atoms were in the metallic (zero) oxidation state, consistent with the observed XPS Pt 4f core level shift. Upon deposition of the Pt nanoparticles, the Raman line shapes and relative D-to-G band intensities remained unchanged. The presence of these peaks verified that the MWNTs remained largely intact during sonochemical treatment and after deposition of the Pt nanoparticles.

The XPS Pt $4f_{7/2}$ core level of the Pt-CNT (not shown; prepared using a 2-hr sonochemical treatment), referencing the graphitic C 1s orbital at a BE equal to 284.4 eV (Ago et al., 1999;

Suzuki et al., 2002), had a BE= 71.4 eV, indicating that Pt was predominantly in the metallic (zero) oxidation state (Fleisch et al., 1986). XPS signals from the C 1s and O 1s and Pt 4f levels and from no other elements were observed. The asymmetry observed in the $4f_{5/2}$ level at ~78 eV indicated a small population of PtO or PtO_2, which was masked by much larger signal from metallic Pt. The lack of insufficient signal from the Pt oxide (PtO_x) hampered precise determination of the stoichiometric proportions of PtO and PtO_2. Hence, EXAFS was needed for clearer structural elucidation.

In comparing the FTs of the EXAFS Pt L_{III} edge of Pt nanoparticles deposited on the –COO- and –C=O functionalized MWNTs, the first nearest neighbor atom was observed at ~1.78 Å in the Pt-MWNT sample instead of the expected distance of ~2.78 Å for Pt-Pt interactions in its zero oxidation state (Fig. 3A). The latter distance was observed for a standard PtO_2 powder used for comparison. This result was consistent with the XPS core level shift for the Pt $4f_{7/2}$ orbital observed at 71.4 eV, denoting metallic Pt (Fleisch et al., 1986). The low *R* value feature at *R* = 1.01 Å was an artifact of imperfect background subtraction due to the intense Pt L_{III} white line at the absorption edge. The dotted line spectrum was that of the reference foil, obtained in the transmission mode for comparison. The strong peaks between 2 and 3 Å correspond to the interaction occurring between the first nearest neighbor (1NN) Pt atoms. Peak positions of the FT at *R*=2.12 and 2.70 Å were in good agreement with positions observed by others for Pt foil (Frenkel et al., 2001; Zhang et al., 2004). In comparing *R* values of Pt-MWNT samples, the predominant 1NN interaction in these samples was

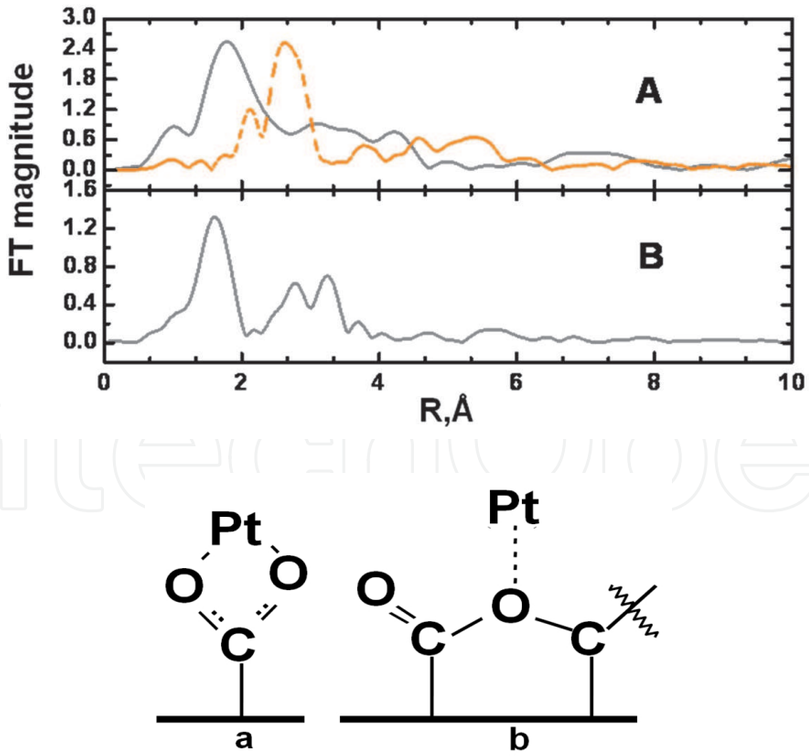

Fig. 3. FTs of EXAFS oscillations plotted in R space of (A) Pt-CNTs (solid gray line; a Pt foil scan is shown as a dotted, orange spectral line); (B) PtO_2 standard; and proposed (a) and (b) structures for Pt-MWNT coordination.

clearly not with Pt-Pt, denoted by the ~1.78 Å position. A FT of a reference PtO_2 powder is shown in Fig. 3B. The location of its 1NN, signifying Pt-O, is seen at R =1.59 Å. EXAFS and XPS data indicated the presence of PtO_x on the Pt-MWNT surface, but not in the bulk of the nanoparticles.

Fig. 4 shows ATR-IR difference spectra of 2 hr sonochemically treated carbon nanotubes before and after Pt nanoparticles were tethered to these surfaces. The C-O ester features, denoted by peaks (2) and (3) in the 2-hr sonicated MWNTs with no Pt deposited, were replaced by a broad single band with a center at 1092 cm^{-1} after Pt nanoparticle attachment. This change in IR envelope shape indicated a strong interaction of ester O with the Pt nanoparticles. The carbonyl O band at 1700 cm^{-1} (before Pt nanoparticle deposition) were replaced by two peaks absorbing at 1712 and 1629 cm^{-1}, indicative of Pt nanoparticles interactions with carbonyl O. Pt binding with the carbonyl O was evident from the absorbance shift from a single feature at 1700 cm^{-1} to two peaks at 1712 and 1629 cm^{-1}. Bands from the ester C-O stretches were still present with vibrational stretches at 1160 cm^{-1}. From *Fig. 4*, it was clear that the Pt loading of the oxidized MWNTs dramatically altered the absorbance signal from the C-O stretches in the 1300-to-900 cm^{-1} region. The carbonyl C=O signal at 1700 cm^{-1} was less affected although there was a shift to higher frequency at 1712 cm^{-1} along with the emergence of another stretch at 1629 cm^{-1}, indicative of multiple binding sites for the Pt nanoparticles. Hence, ATR-IR data showed that the ester O peaks present before tethering Pt nanoparticles were radically altered after the Pt deposition, denoting their involvement in the coordination of the Pt nanoparticles to create the nanostructure. Based on this IR result and the EXAFS analysis, we propose two Pt-MWNT surface structures. Attachment can occur via carboxylate ions in which the O atoms effectively have equal bond order and participation in the Pt binding in the form of COO(Pt) (Fig. 3a). Pt nanoparticles can also coordinate to ester O atoms bound to the carbon nanotube surface, bridging between two carbons and serving as a binding site for the Pt nanoclusters in the form of C(=O)CO(Pt) (Fig. 3b). According to Petroski and El-Sayed (2003), because the d band of Pt is close to the Fermi level, electron density to form new bonds would come from the C=O group rather than the Pt. Hence, shifts in the C=O stretch would be sensitive to coordination with Pt (peak 1 in Fig. 4) as observed.

In our final case study, variations in the measured PZC were seen between differently functionalized SWNT structures (McPhail et al., 2009). Fig. 5 shows a plot of final versus initial pH values of solutions to which various SWNT samples were added. A plateau (horizontal dashed lines) in the plot indicates the PZC for each specifically-functionalized carbon nanotube.

The PZC values in this series of functionalized carbon nanotubes indicated a relatively acidic surface, amenable for adsorption of anionic (metal nanoparticle) precursors. The PZC values for the SWNTs were in ascending order: COOH-SWNTs (1.2) < MA-SWNTs (2.0) < p-SWNTs (3.5) < NO-SWNTs (7.5). Lowering of the p-SWNTs PZC compared to other studies (Matarredona et al., 2003) was attributed to our use of smaller radius (~0.7 nm) SWNTs. The COOH groups, due to its acidity, lowered the PZC to a greater extent than the MA groups (by 0.8 pH units). The PZCs were found to be tunable within 6.3 pH units by functionalizing them with various moieties of different electron withdrawing/donating character. The moieties markedly affected the PZCs. There is an obvious correlation of PZC with electron distribution, emanating from attached moieties along the SWNTs sidewalls.

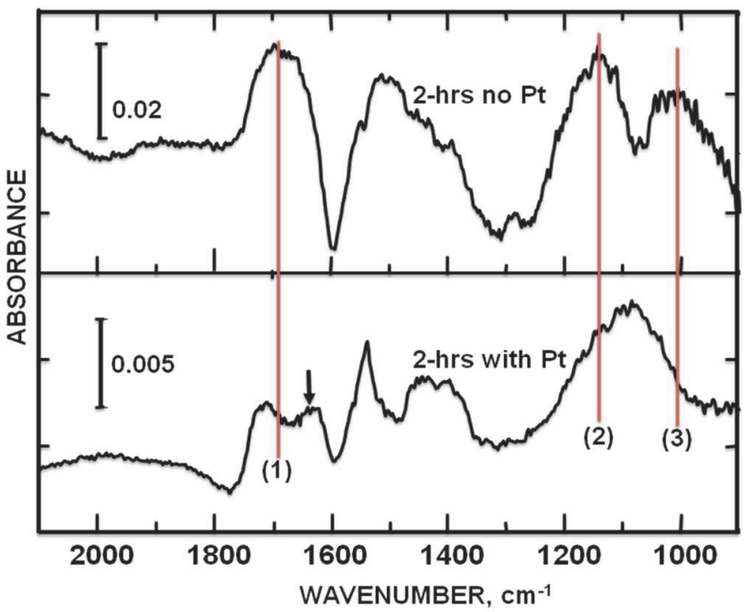

Fig. 4. ATR-IR difference spectra of 2100-900 cm^{-1} region of 2-hr sonochemically treated carbon nanotubes before and after Pt nanoparticle deposition. Untreated carbon nanotubes were used for background subtraction. Vibrations from (1) carbonyl and ester (2) asymmetric and (3) symmetric stretches are noted for comparison. The arrow denotes a new frequency signifying coordination with Pt nanoparticles.

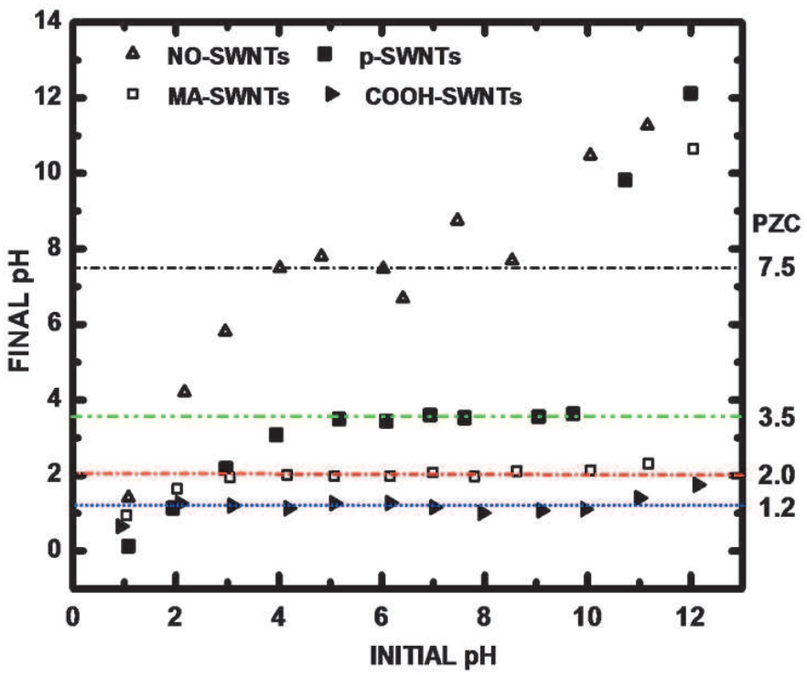

Fig. 5. The point of zero charge (PZC) values of NO-SWNTs, p-SWNTs, MA-SWNTs and COOH-SWNTs are denoted by horizontal lines.

In the context of electrophilic aromatic substitution (EAS) reactions, nitroso groups are known to be electron withdrawing, maleic anhydride groups are lightly electron releasing, and carboxylic acid groups are strongly electron releasing, which can be quantitatively described by Hammett sigma constants (σ). Since carbon nanotubes are essentially aromatic, peri-condensed benzenoids (composed of sp^2 carbons, arranged in a graphite-like hexagonal pattern) that have aromatic character (Linert et al., 2007; Lukovits et al., 2007) and are used to fabricate hierarchical structures (Zorbas et al., 2005), it is appropriate to explore how σ relates to our observed PZC measurements. Also known as the "substituent constant," σ determines the effect that a given substituent will have on the equilibrium and rate constants for the disassociation of benzoic acids. The σ parameter takes into account resonance, field, and inductive effects of the substituent. The result is a value whose magnitude gives the relative strength of a substituent's effect on the electronic distribution of a benzoic acid. Standard tables show σ values (for the meta- position) of 0.71, 0.39, and 0.35 for nitro, acetoxy, and carboxylic acid groups, respectively (Hansch et al., 1991; Carey, 2002). Larger σ values denote greater electron-withdrawing character. The MA and COOH groups, which are the least electron withdrawing (i.e., more electron releasing) lowered the PZC, relative to p-SWNTs, while NO, the most electron withdrawing moiety, raised the PZC. Variations in the electron releasing/withdrawing character of the substituents correlate well with the observed PZC trend. In our previous work (McPhail et al., 2009), we postulated that the PZC was dependent on SWNT electronic structure.

Here, we note a new observation: greater σ values coincide with a greater propensity to be hydroxylated, thereby increasing the PZC. The greater electron donating character of the moiety led to an increased degree of surface hydroxylation. Quantitatively, the σ values of the substituents show the same increasing trend as that of the experimentally measured PZCs for each corresponding, functionalized SWNT (Fig. 5).

4. Conclusions

In summary, we have demonstrated the utility of XPS for delineating MWNT oxidation kinetics, EXAFS (coupled with XPS and ATR-IR) for elucidating nanoparticle-MWNT interfacial structure, and the dependence of PZC on the electron withdrawing/donating character of moieties attached to SWNTs. Sonication of MWNTs is a facile functionalization technique as it lowers the surface activation energy barrier resulting in low temperature functionalization and reduction in surface physical damage. The process greatly reduces the functionalization time to as low as 2 hrs. Sonochemical treatments tend to create dangling bonds on the surfaces of carbon nanotubes, which progressively oxidize to hydroxyl (OH), carbonyl (CO), and carboxyl (COOH) functional groups (Al-Aqtash and Vasiliev, 2009). Kinetic studies uncovered a stochastic functionalization mechanism involved in the preparation of MWNTs for nanoparticle attachment. EXAFS, coupled with XPS and ATR-IR data, was pivotal in the elucidation of ester-like O atoms found to play an important role in synthesizing Pt nanoparticle-MWNT structures. Controlled surface functionalization on SWNTs can influence its PZC, an important variable for Coulombic attachment of structures onto the surface. The above described surface analytical methods, performed on MWNTs and SWNTs as benchmarks, may well be applicable for examining aqueous solution functionalization processes on newly emerging carbon nanomaterials, i.e., graphene and

graphene oxides (Liu et al., 2008; Geim, 2009; Yan and Chou, 2010), for advanced technological applications.

5. Acknowledgements

We gratefully acknowledge support from the Faculty Research Creative Activity Committee (FRCAC) of Middle Tennessee State University awarded in 2011.

6. References

Ago, H.; Kugler, T.; Cacialli, F.; Salaneck, W. R.; Shaffer, M. S. P.; Windle, A. H.; Friend, R. H. (1999). Work Functions and Surface Functional Groups of Multiwall Carbon Nanotubes. *J. Phys. Chem. B*, 103, 8116-8121.

Al-Aqtash, N.; Vasiliev, I. Y. (2009). Ab initio Study of Carboxylated Graphene. *J. Phys. Chem. C,* 113, 12970-12975.

Brown, G.E., Jr.; Henrich, V.E.; Casey, W.H.; Clark, D.L.; Eggleston, C.; Felmy, A.; Goodman, D.W.; Grätzel, M.; G. E. Maciel; McCarthy, M.I.; Nealson, K.; Sverjensky, D.A.;Toney, M.F.; Zachara, J.M. (1999) Chemical Interactions of Metal Oxide-Aqueous Solution Interfaces," *Chem. Rev.*, 99, 77-174.

Brukh, R.; Mitra, S. (2007). Kinetics of Carbon Nanotube Oxidation. *J. Mater. Chem.*, 17, 619-623.

Carey, F. A. (2002). *Advanced Organic Chemistry, Part A: Structure and Mechanisms*, 4th ed.; Kluwer Academics/Plenum Publishers: New York.

Chen, G.-X.; Kim, H.-S.; Park, B. H.; Yoon, J.-S. (2005). Controlled Functionalization of Multiwalled Carbon Nanotubes with Various Molecular-Weight Poly (l-lactic acid). *J. Phys. Chem. B*, 109, 22237-22243.

Chiang, Y.-C.; Lin, W.-H.; Chang, Y.-C. (2011). The Influence of Treatment Duration on Multi-walled Carbon Nanotubes Functionalized by H_2SO_4/HNO_3 Oxidation. *Appl. Surf. Sci.,* 257, 2401-2410.

Dai, H. (2002). Carbon Nanotubes: Synthesis, Integration, and Properties. *Acc. Chem. Res.*, 35, 1035-1044.

Datsyuk, V.; Kalyva, M.; Papagelis, K.; Parthenios, J.; Tasis, D.; Siokou, A.; Kallitsis, I.; Galiotis, C. (2008). Chemical Oxidation of Multiwalled Carbon Nanotubes. *Carbon*, 46, 833-840.

Dewar, M. J. S.; Pyron, R. S. (1970). Nature of the Transition State in Some Diels-Alder Reactions. *J. Am. Chem. Soc.*, 92, 3098-3103.

Ebbesen, T.W.; Lezec, H.J.; Hiura, H.; Bennett, J.W.; Ghaemi, H.F.; Thio, T. (1996). Electrical Conductivity of Individual Carbon Nanotubes. *Nature*, 382, 54-56.

Fleisch, T. H.; Mains, G. J. (1986). Photoreduction and Reoxidation of Platinum Oxide Surfaces. *J. Phys. Chem.*, 90, 5317-5320.

Frenkel, A. I.; Hills, C. W.; Nuzzo, R. G. (2001). A View from the Inside: Complexity in the Atomic Scale Ordering of Supported Metal Nanoparticles. *J. Phys. Chem. B*, 105, 12689-12703.

Geim, A.K. (2009). Graphene: Status and Prospects. *Science*, 324, 1530-1534.

Hansch, C.; Leo, A.; Taft, R. W. (1991). A Survey of Hammett Substituent Constants and Resonance and Field Parameters. *Chem. Rev.*, 91, 165–195.

Holzinger, M., Vostrowsky, O., Hirsch, A., Hennrich, F., Kappes, M., Weiss, R.; Jellen, F. (2001). Sidewall Functionalization of Carbon Nanotubes. *Ang. Chem. Inter. Ed.*, 40, 4002–4005.

Huefner, S. (2003). *Photoelectron Spectroscopy*, Springer: Berlin.

Hull, R. V.; Li, L.; Xing, Y.; Chusuei, C. C. (2006). Pt Nanoparticle Binding on Functionalized Multiwalled Carbon Nanotubes. *Chem. Mater.*, 18, 1780-1788.

Iijima, S. (1991). Helical Microtubules of Graphitic Carbon. *Nature*, 354, 56-58.

Kam, N.W.S.; O'Connell, M.; Wisdom, J.; Dai, H. (2005). Carbon Nanotubes as Multifunctional Biological Transporters and Near-infrared Agents for Selective Cancer Cell Destruction." *Proc. Natl. Acad. Sci. U.S.A.*, 102, 11600-11605.

Kim, B.; Sigmund, W. M. (2004). Functionalized Multiwall Carbon Nanotube/Gold Nanoparticle Composites. *Langmuir*, 20, 8239-8242.

Kojima, I.; Miyazaki, E.; Iwao, Y. (1982). Field Emission Study of VIII Transition Metals. III. Adsorption of Ethylene and Acetylene on Platinum. *Appl. Surf. Sci.*, 10, 27-41.

Lamber, R.; Jaeger, N.I. (1993). Electron Microsopy Study of the Interaction of Nickel, Palladium and Platinum with Carbon. III: Formation of a Substitutional Platinum-carbide in Ultrafine Platinum Particles. *Surf. Sci.*, 289, 247-254.

Langley, L. A.; Villanueva, D. E.; Fairbrother, D. H. (2005). Quantification of Surface Oxides on Carbonaceous Materials. *Chem. Mater.*, 18, 169-178.

Li, J.-L.; Kudin, K. N.; McAllister, M. J.; Prud'homme, R. K.; Aksay, I. A.; Car, R. (2006). Oxygen-Driven Unzipping of Graphitic Materials. *Phys. Rev. Lett.*, 96, 176101.

Linert, W.; Lukovits, I. (2007). Aromaticity of Carbon Nanotubes. *J. Chem. Info. Model.*, 47, 887-890.

Liu, L.; Ryu, S.; Tomasik, M. R. ;Stolyarova, E.; Jung, N.; Hybertsen, M. S.; Steigerwald, M. L.; Brus, L. E. and Flynn, G.W. (2008). Graphene Oxidation: Thickness-Dependent Etching and Strong Chemical Doping. *Nano Lett.*, 8, 1965-1970.

Lu, X.; Imae, T. (2007). Size-Controlled In Situ Synthesis of Metal Nanoparticles on Dendrimer-Modified Carbon Nanotubes. *J. Phys. Chem. C*, 111, 2416-2420.

Lukovits, I.; Kármán, F.; Nagy, P.M.; Kálmán, E. (2007). Aromaticity of Carbon Nanotubes. *Croat. Chem. Acta*, 80, 233–237.

Matarredona, O.; Rhoads, H.; Li, Z.; Harwell, J. H.; Balzano, L.; Resasco, D. E. (2003). Dispersion of Single-Walled Carbon Nanotubes in Aqueous Solutions of the Anionic Surfactant NaDDBS. *J. Phys. Chem. B*, 107, 13357-13367.

Mawhinney, D.B.; Naumenko, V.; Kuznetsova, A.; Yates, J., John T. (2000). Infrared Spectral Evidence for the Etching of Carbon Nanotubes: Ozone Oxidation at 298 K. *J. Am. Chem. Soc.*, 122, 2383-2384.

McPhail, M.R.; Sells, J.A.; He, Z.; Chusuei. C. C. (2009). Charging Nanowalls: Adjusting the Carbon Nanotube Isoelectric Point via Surface Chemical Functionalization. *J. Phys. Chem. C*, 113, 14102-14109.

Mercuri, F.; Sgamellotti, A. (2009). First-principles Investigations on the Functionalization of Chiral and Non-chiral Carbon Nanotubes by Diels-Alder Cycloaddition Reactions. *Phys. Chem. Chem. Phys*., 11, 563-567.

Newville, M. (2001). IFEFFIT: Interactive XAFS Analysis and FEFF Fitting. *J. Synch. Rad.*, 8, 322-324.

Okpalugo, T. I. T.; Papakonstantinou, P.; Murphy, H.; McLaughlin, J.; Brown, N. M. D. (2005). High Resolution XPS Characterization of Chemical Functionalised MWCNTs and SWCNTs. *Carbon*, 43, 153-161.

Park, J.; Regalbuto, J. R. (1995). A Simple, Accurate Determination of Oxide PZC and the Strong Buffering Effect of Oxide Surfaces at Incipient Wetness. *J. Colloid Inter. Sci.*, 175, 239-252.

Park, M. J.; Lee, J. K.; Lee, B. S.; Lee, Y.-W.; Choi, I. S.; Lee, S.-g. (2006). Covalent Modification of Multiwalled Carbon Nanotubes with Imidazolium-Based Ionic Liquids: Effect of Anions on Solubility. *Chem. Mater.*, 18, 1546-1551.

Petroski, J.; El-Sayed, M.A. (2003). FTIR Study of the Adsorption of the Capping Material to Different Platinum Nanoparticle Shapes. *J. Phys. Chem. A*, 107, 8371-8375.

Planeix, J.M.; Coustel, N.; Coq, B.; Brotons, V.; Kamblar, P.S.; Dutartre, R.; Geneste, P.; Bernier, P.; Ajayan, P.M. (1994). Application of Carbon Nanotubes as Supports in Heterogeneous Catalysis. *J. Am. Chem. Soc*., 116, 7935-7936.

Poh, W. C.; Loh, K. P.; Zhang, W. D.; Sudhiranjan; Ye, J.-S.; Sheu, F.-S. (2004). Biosensing Properties of Diamond and Carbon Nanotubes. *Langmuir*, 20, 5484-5492.

Ravel, B.; Newville, M. (2005). ATHENA, ARTEMIS, HEPHAESTUS: Data Analysis for X-ray Absorption Spectroscopy Using IFEFFIT. *J. Synchrotron Radiat.*, 12, 537-541.

S. Lee, et al. (2010). Characterization of Multi-walled Carbon Nanotubes Catalyst Supports by Point of Zero Charge, *Catal. Today*, doi:10.1016/j.cattod.2010.10.031

Suzuki, S.; Watanabe, Y.; Ogino, T.; Heun, S.; Gregoratti, L.; Barinov, A.; Kaulich, B.; Kiskinova, M.; Zhu, W.; Bower, C.; Zhou, O. (2002). Electronic Structure of Carbon Nanotubes Studied by Photoelectron Spectromicroscopy. *Phys. Rev. B*, 66, 035414-1–035414-4.

Wang, Y.; Malhotra, S. V.; Owens, F. J.; Iqbal, Z. (2005). Electrochemical Nitration of Single-wall Carbon Nanotubes. *Chem. Phys. Lett.*, 407, 68-72.

Xing, Y. (2004). Synthesis and Electrochemical Characterization of Uniformly-Dispersed High Loading Pt Nanoparticles on Sonochemically-Treated Carbon Nanotubes. *J. Phys. Chem. B*, 108, 19255-19259.

Xing, Y.; Li, L.; Chusuei, C. C.; Hull, R. V. (2005). Sonochemical Oxidation of Multiwalled Carbon Nanotubes. *Langmuir*, 21, 4185-4190.

Zhang, J.; Hongling, Z.; Qing, Q.; Yang, Y.; Li, Q.; Liu, Z.; Guo, X.; Du, Z. (2003). Effect of Chemical Oxidation on the Structure of Single-Walled Carbon Nanotubes. *J. Phys. Chem. B*, 107, 3712-3718.

Zhang, Y.; Toebes, M. L.; van der Eerden, A.; O'Grady, W. E.; de Jong, K. P.; Koningsberger, D. C. (2004). Formation, Characterization, and Magnetic Properties of Fe_3O_4 Nanowires Encapsulated in Carbon Microtubes. *J. Phys. Chem. B*, 108, 18509-18519.

Zorbas, V.; Smith, A. L.; Xie, H.; Ortiz-Acevedo, A.; Dalton, A. B.; Dieckmann, G.; Draper, R. K.; Baughman, R. H.; Musselman, I. H. (2005). Importance of Aromatic Content for Peptide/Single-walled Carbon Nanotube Interactions. *J. Am. Chem. Soc.*, 127, 12323-12328.

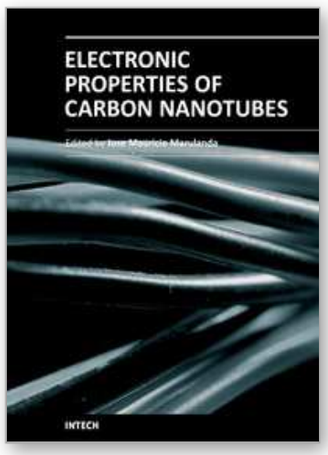

Electronic Properties of Carbon Nanotubes

Edited by Prof. Jose Mauricio Marulanda

ISBN 978-953-307-499-3
Hard cover, 680 pages
Publisher InTech
Published online 27, July, 2011
Published in print edition July, 2011

Carbon nanotubes (CNTs), discovered in 1991, have been a subject of intensive research for a wide range of applications. These one-dimensional (1D) graphene sheets rolled into a tubular form have been the target of many researchers around the world. This book concentrates on the semiconductor physics of carbon nanotubes, it brings unique insight into the phenomena encountered in the electronic structure when operating with carbon nanotubes. This book also presents to reader useful information on the fabrication and applications of these outstanding materials. The main objective of this book is to give in-depth understanding of the physics and electronic structure of carbon nanotubes. Readers of this book should have a strong background on physical electronics and semiconductor device physics. This book first discusses fabrication techniques followed by an analysis on the physical properties of carbon nanotubes, including density of states and electronic structures. Ultimately, the book pursues a significant amount of work in the industry applications of carbon nanotubes.

InTech Europe
University Campus STeP Ri
Slavka Krautzeka 83/A
51000 Rijeka, Croatia
Phone: +385 (51) 770 447
Fax: +385 (51) 686 166
www.intechopen.com

InTech China
Unit 405, Office Block, Hotel Equatorial Shanghai
No.65, Yan An Road (West), Shanghai, 200040, China
中国上海市延安西路65号上海国际贵都大饭店办公楼405单元
Phone: +86-21-62489820
Fax: +86-21-62489821

IntechOpen